

# $C^2$ Splines Covering Polar Configurations

Ashish Myles<sup>a</sup>

<sup>a</sup>*CS Dept, New York University, 715 Broadway, 12th Floor, New York, NY 10003, USA*

Jörg Peters<sup>b</sup>

<sup>b</sup>*CISE Dept, Bldg 42, Rm E301, University of Florida, Gainesville, FL 32611, USA*

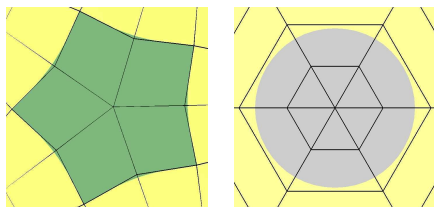
---

## Abstract

A *polar configuration* is a triangle fan in a quad-dominant mesh; it allows for many mesh lines to join at a single polar vertex. This paper shows how a single tensor-product spline of degree (3, 6) can cap a polar configuration with a  $C^2$  surface. By design, this  $C^2$  polar spline joins  $C^2$  with surrounding bi-3 tensor-product splines and thereby complements algorithms that smoothly cap star-like, multi-sided regions.

*Key words:*  $C^2$ , polar, spline, B-spline, curvature-continuous

---



(a) star-like layout      (b) Polar layout

Fig. 1. (a) A star-like mesh-configuration covered by  $n$  patches. (b) A polar configuration covered by one polar spline.

## 1. Motivation

CAD modeling systems represent parametric surfaces by a finite number of quadrilateral spline patches in tensor-product B-spline form. To generate surfaces of arbitrary genus in this representation, a number of algorithms have been devised that smoothly complete a piecewise bicubic  $C^2$  surface, by filling-in star-like, multi-sided holes with  $n$  patches as in Fig. 1. But, as pointed out for example in [KP07a], these constructions are not well-suited for high-valence neighborhoods arising from extruded, high-valent or periodic features as in Fig. 2 and 11. Where many patches come together, it is more natural to have a triangle fan join many parameter lines at a common *pole* similar to the latitude/longitude connectivity at the poles of the earth. If

such a polar multi-sided hole is to be covered by subdivision, [MP09] gives simple rules that create a  $C^2$  completion of degree 3. But, except for display, subdivision algorithms do not readily fit into the major CAD modeling frameworks. We therefore develop a new  $C^2$  Polar Spline that, for a polar configuration,

- consists of one tensor-product spline of degree (3,6),
- is easy to construct, by formulas (4)(5)(6) of Section 6,
- is easy to analyze, and
- is *bi-3  $C^2$  compatible*, that is, meets  $C^2$  with surrounding  $C^2$  bi-3 tensor-product splines.

In more detail, the  $C^2$  Polar Spline is of degree 6 in the periodic direction and of degree 3 in the radial direction. One boundary is collapsed to a single point  $\mathbf{p}_0$ , the pole (cf. Fig. 3 and 6c). Since the spline is  $C^2$ , the degree 6 periodic direction has 4-fold knots. The knots in the radial direction are repeated so that  $\mathbf{p}_0$  is interpolated. The spline is derived by explicitly relating its control points to a second-order expansion of the surface at the pole in a special shape basis.

*Overview* After reviewing related literature, formally stating the challenge, pointing to observations that enable the construction and laying out the tools (Sections 2–5), we formally state the algorithm in Section 6. Section 7 proves curvature continuity and bi-3  $C^2$  compatibility of  $C^2$  polar splines. Section 8 explains what alternative constructions are possible and why we chose the particular set of rules. Section 9 explores the relation of polar splines to

---

*Email addresses:* amyles@cs.nyu.edu (Ashish Myles), jorg@cise.ufl.edu (Jörg Peters).

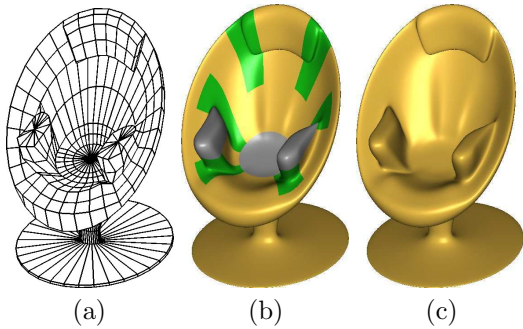


Fig. 2. **Polar Chair.** (a) A mesh with three polar configurations (arm-rests, center), as well as star-like (Catmull-Clark-type) extraordinary vertices, defines a smooth manifold (c) consisting of a small number of tensor-product splines. (b) Uniform bi-3 splines are *gold*,  $C^2$  polar splines are *gray*; star-like-neighborhoods can be covered by, for example, by one of [Pra97, KP09b, LS08] (*green*).

polar subdivision. Section 10 concludes with a gallery of shapes and its discussion.

## 2. Related work

A number of constructions yield curvature-continuous free-form surfaces from coarse control meshes, for example [Pra97, Rei98, Pet02, YZ04, Lev06, KP07b, KP09b, LS08]. Techniques that generate  $C^2$  spline surfaces on arbitrary quad meshes include Prautzsch’s free-form splines [Pra97] and Reif’s TURBS [Rei98], both of degree bi-6; Karčiauskas and Peters’ guided spline surfaces [KP07b, KP09b]; and Loop and Schaefer’s bi-7 construction [LS08], improving [Loo04]. Ying and Zorin’s approach [YZ04] generates surfaces from quad meshes by joining locally-defined polynomials via exponential blending functions. Bohl and Reif [BR97] use a careful reparameterization to analyze constructions with multiple collapsed layers of control points. All above constructions represent parametric surfaces by a finite number of patches.

Quad-based subdivision algorithms, while enabling free-form modeling with simple implementations, do not readily fit into this framework. And it has proven difficult to generate  $C^2$  surfaces based on subdivision for star-like configurations. Levin [Lev06] blended Catmull-Clark subdivision surfaces near extraordinary vertices with polynomials to produce curvature continuity at extraordinary points. For triangle meshes, Zorin [Zor06] similarly blended Loop subdivision surfaces with polynomials, but used blending functions that were themselves subdivision surfaces. At present, we are unaware of any *simple* subdivision algorithms for covering star-like holes by a  $C^2$  surface cap.

For polar configurations, Karčiauskas et al. [KMP06] defined a  $C^2$  surface consisting of an infinite sequence of surface rings of degree (5, 6) and Myles and Peters improved on this with a bi-3  $C^2$  subdivision construction with simple rules [MP09]. The corresponding limit surface consists of an infinite sequence of polynomial surface rings. The  $C^2$  polar splines constructed below provide a finite CAD-friendly counterpart to this algorithm. Another finite construction,

Table 1

**The shape basis.** Our choice (4) of  $\mathbf{v}$  and change of parameterization from (b)→(c) produce the shape basis (c). When converted to polar coordinates (d), each basis in function (c) belongs to exactly one Fourier frequency (e).

$k$	$h_{\mathbf{v}_k}(r, \gamma)$	reparam.	polar coord.	$\theta$ freq.
0	1	1	1	0
1	$r f_{\mathbf{v}_1}(\gamma)$	$x$	$\rho \cos(\theta)$	1
2	$r f_{\mathbf{v}_2}(\gamma)$	$y$	$\rho \sin(\theta)$	1
3	$r^2(f_{\mathbf{v}_1}^2(\gamma) + f_{\mathbf{v}_2}^2(\gamma))$	$x^2 + y^2$	$\rho^2$	0
4	$r^2(f_{\mathbf{v}_1}^2(\gamma) - f_{\mathbf{v}_2}^2(\gamma))$	$x^2 - y^2$	$\rho^2 \cos(2\theta)$	2
5	$r^2(2f_{\mathbf{v}_1}(\gamma)f_{\mathbf{v}_2}(\gamma))$	$2xy$	$\rho^2 \sin(2\theta)$	2
(a)	(b)	(c)	(d)	(e)

with  $n$  Bézier patches of degree (6,5) appeared in [KP09a]. This pairing of subdivision with a finite patch construction is analogous to pairing bi-3 polar subdivision with a bi-3 spline  $C^1$  construction in [MKP08]. (Section 9 describes an alternative bi-3 spline derived from the new framework that has fewer control points.)

## 3. Polar configurations and $C^2$ expansions

A  $k$ -layer **polar configuration** is a submesh consisting of a triangle fan surrounded by  $k$  layers of quads that have only 4-valent vertices (see Figure 6a). The central vertex of the triangle fan is the *polar vertex*, and its valence is denoted  $n$ . The corresponding point on the spline surface is the *pole*. A designer can easily separate a polar vertex from another polar vertex or a star-like configuration by adding an edge loop encircling the polar vertex.

Two layers of control points in the vicinity of the polar vertex will determine the second-order expansion of the surface at the pole. The control points will be linearly combined to create control points in the following *shape basis* of polynomials of order 2:

$$\mathbf{s} := [1, x, y, x^2 + y^2, x^2 - y^2, 2xy]. \quad (1)$$

The shape basis is similar both to the power-form expansion and to the expansion in polar coordinates  $(x, y) = (\rho \cos(\theta), \rho \sin(\theta))$ . Table 1(c,d) shows how each basis function in  $\mathbf{s}$  corresponds to exactly one  $\theta$  frequency. Thus, defining a quadratic surface as

$$\mathbf{p}_0 + \mathbf{p}_1 x + \mathbf{p}_2 y + \mathbf{p}_3(x^2 + y^2) + \mathbf{p}_4(x^2 - y^2) + \mathbf{p}_5(2xy) \quad (2)$$

gives  $\mathbf{p}_0, \mathbf{p}_1, \mathbf{p}_2, \mathbf{p}_3, \mathbf{p}_4, \mathbf{p}_5 \in \mathbb{R}^3$  the intuitive geometric meaning illustrated in Figure 3:

- $\mathbf{p}_0$  is a point on the surface;
- $\mathbf{p}_1$  and  $\mathbf{p}_2$  help span the tangent plane;
- $\mathbf{p}_3$  determines the ellipticity; and
- $\mathbf{p}_4$  and  $\mathbf{p}_5$  together define the orientation and magnitude of the saddle components.

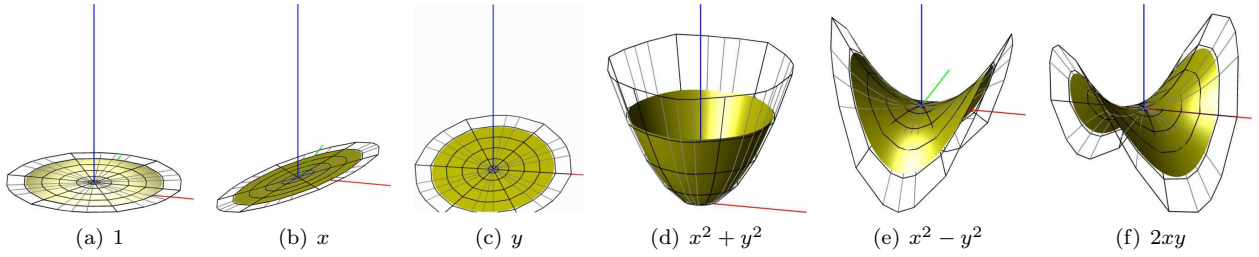


Fig. 3. **The shape basis** represents geometric properties of the surface: (a) position, (b and c) tangent plane, (d) elliptic, and (e and f) hyperbolic expansion terms. The control nets are defined by (16).

#### 4. Observations that enable the construction

First, consider a quad mesh with polar configurations converted to bi-3 splines except for surface ‘caps’ defined by star-like and polar configurations. Figure 1 illustrates how a corresponding polar cap is surrounded by a single smooth curve while the star-like cap’s boundary is a zigzag curve. Correspondingly, the polar cap can be a single, parametrically  $C^2$ , periodic spline patch whose outer boundary matches the boundary of the polar configuration; while star-like caps consist naturally of  $n$  patches with distinct parameterization that may be joined with geometric, namely  $G^2$  continuity.

Secondly, we can approximate the disk  $(\rho \cos(\theta), \rho \sin(\theta))$ ,  $\rho \in [0..1]$ ,  $\theta \in [0..2\pi]$  by a  $C^2$  periodic polynomial spline  $(u, v) \rightarrow (x, y)$  that is of degree 1 in the *radial direction* emanating from the polar vertex and of degree 3 in the *periodic direction* approximating sine and cosine variation. No less than degree 3 will do if we require parametric  $C^2$  continuity in the periodic direction. Consequently, the space of quadratic functions  $z(x, y)$

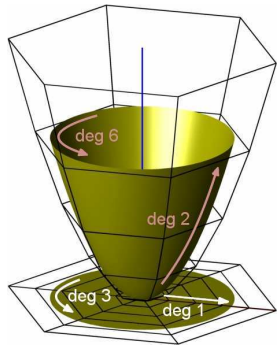


Fig. 4.  $C^2$  polar splines require degree (2,6) to represent graphs of quadratics.

includes maps of degree (2,6) in the spline parameters. This is illustrated in Fig. 4 and was also shown in [MP09].

Finally, as displayed in Table 1(d), each function in the basis  $\mathbf{s}$  can be viewed as a radial function tensored with a periodic function. Section 5 gives a specific choice of univariate periodic degree 3 splines,  $f_{v_1}(\gamma)$  and  $f_{v_2}(\gamma)$ , that approximate  $\cos(2\pi\gamma/n)$  and  $\sin(2\pi\gamma/n)$ , respectively. Then parameterizing  $(x, y) = (rf_{v_1}(\gamma), rf_{v_2}(\gamma))$  yields the factored basis functions of degree (3,6) of  $\mathbf{s}$  in Table 1(b) that are suitable for parameterizing the neighborhood of the pole as shown in Figure 3. (The precise degree to which cosine and sine are approximated is irrelevant for curvature continuity as the proof in Section 7 only relies on the reparameterization above being valid – i.e. a diffeomorphism away from the origin.)

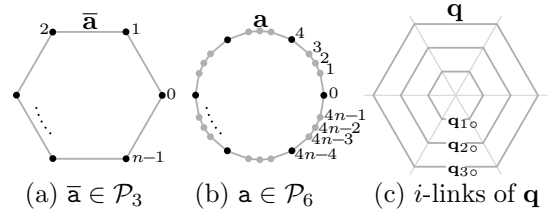


Fig. 5. **Notation.** (a) A periodic control polygon with  $n$  coefficients of a degree 3 spline with uniform knots. (b) A periodic control polygon with  $4n$  coefficients of a degree 6 spline with 4-fold knots. (c) Periodic  $i$ -links of a polar configuration (in thick gray).

#### 5. $C^2$ Polar Spline Basics

As illustrated in Fig. 6, we will fit one periodic spline to each polar configuration in the quad mesh. Since we construct the spline independently in each coordinate, we distinguish vectors in  $\mathbb{R}^3$  using boldface, e.g.  $\mathbf{q}_{ij}$ ,  $\mathbf{b}_{ij}$ ,  $\mathbf{p}_k \in \mathbb{R}^3$ , from scalars representing one coordinate, using teletype:  $q_{ij}$ ,  $b_{ij}$ ,  $p_k \in \mathbb{R}$ . We want to tensor univariate radial and periodic functions in the bases of Table 1b. Therefore, in the radial direction, the algorithm will generate the functions  $\{1, r, r^2\}$  using cubic splines and, in the periodic direction, the splines

$$(f_{v_0}, f_{v_1}, f_{v_2}, f_{v_3}, f_{v_4}, f_{v_5}) := \quad (3)$$

$$(1, f_{\bar{v}_1}, f_{\bar{v}_2}, f_{\bar{v}_1}^2 + f_{\bar{v}_2}^2, f_{\bar{v}_1}^2 - f_{\bar{v}_2}^2, 2f_{\bar{v}_1}f_{\bar{v}_2})$$

based on univariate periodic splines  $f_{\bar{v}_1}$  and  $f_{\bar{v}_2}$  of degree 3 that approximate cosine and sine. To define the periodic functions, we use the following notation.

**Univariate periodic splines:** Let  $n$  be the valence of the polar vertex. Let  $\mathcal{P}_k$  be the *space of control polygons* of periodic  $C^2$  splines with uniformly-spaced knots of multiplicity  $k - 2$  (Figure 5a–b). We define a  $C^2$  periodic *spline* of degree  $d$ ,  $d > 2$ ,

$$f_{\mathbf{a}} : [0, 1] \rightarrow \mathbb{R}, \quad \mathbf{a} \in \mathcal{P}_d := \mathbb{R}^{(d-2)n}$$

by uniformly-spaced,  $(d-2)$ -fold knots at the integers modulo  $n$  scaled down by  $n$ ,  $\frac{1}{n}\mathbb{Z}_n$ , and control points  $\mathbf{a}$  with periodic repetition. That is, for  $d = 3$  the knot sequence is just  $\frac{1}{n}\mathbb{Z}_n$  and for  $d = 6$ ,

$$\frac{1}{n}[0, 0, 0, 0, 1, 1, 1, 1, \dots, n-1, n-1, n-1, n-1].$$

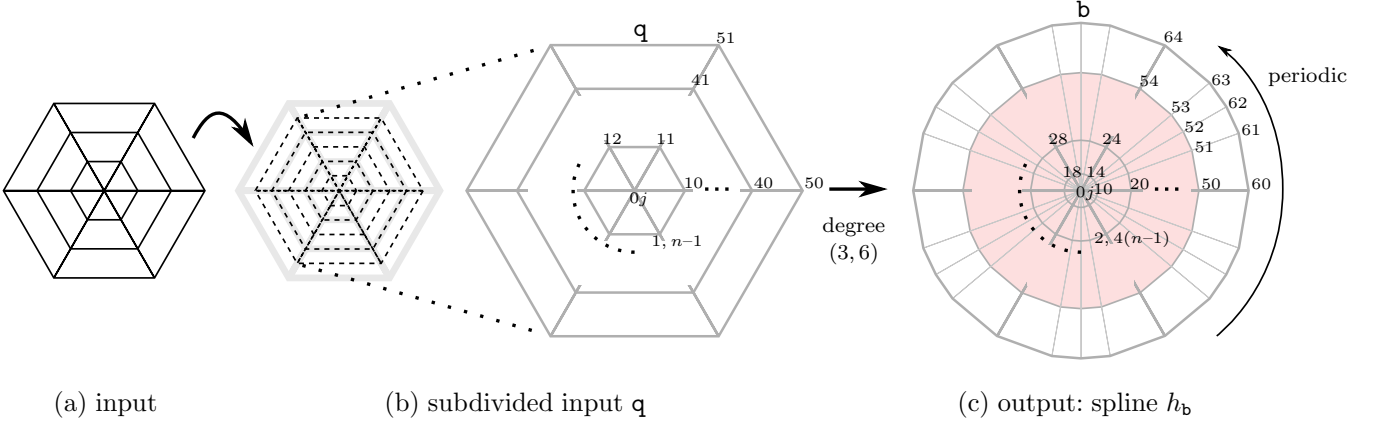


Fig. 6. **Construction of the  $C^2$  polar spline.** (a) A 2-layer polar configuration is once-refined by bicubic polar subdivision [MKP08] to yield (b) the 4-layer configuration  $\mathbf{q}$ . From  $\mathbf{q}$ , the construction derives (c) the control points  $\mathbf{b}$  of the spline  $h_{\mathbf{b}}$  (pink) of degree  $(3, 6)$ .

**$i$ -link:** We define the  $i$ -link of a polar configuration  $\mathbf{q}$  to be a  $n$ -vector of vertices that are  $i$  radial edges away from the polar vertex  $\mathbf{q}_{i\circ} := [\mathbf{q}_{ij}]_{j \in \mathbb{Z}_n}$  (Fig. 5c). The vector  $\mathbf{q}_{i\circ}$  can be interpreted as an element of  $\mathcal{P}_3$ .

**Spline multiplication:** The operator  $\diamond : \mathcal{P}_3 \times \mathcal{P}_3 \rightarrow \mathcal{P}_6$  expresses spline multiplication in terms of the control points:

$$f_{\bar{\mathbf{a}}_1} f_{\bar{\mathbf{a}}_2} = f_{\bar{\mathbf{a}}_1 \diamond \bar{\mathbf{a}}_2} \quad \text{for } \bar{\mathbf{a}}_1, \bar{\mathbf{a}}_2 \in \mathcal{P}_3.$$

In particular, if  $\mathbf{1} \in \mathcal{P}_3$  is the vector of all 1s,  $\bar{\mathbf{a}} \diamond \mathbf{1} \in \mathcal{P}_6$ , and  $f_{\bar{\mathbf{a}} \diamond \mathbf{1}}$  is the degree-raised representation of  $f_{\bar{\mathbf{a}}}$ . The Appendix gives explicit formulas and code to implement the  $\diamond$  operator. This and weighted vector addition are the only operations needed for implementing  $C^2$  polar splines.

**Periodic bases  $f_{\mathbf{v}_k}$ :** Cosine and sine can be approximated by a pair of degree 3 splines  $f_{\bar{\mathbf{v}}_1}$  and  $f_{\bar{\mathbf{v}}_2}$  with coefficients  $\bar{\mathbf{v}}_1, \bar{\mathbf{v}}_2 \in \mathcal{P}_3$ ,

$$(\bar{\mathbf{v}}_1)_j := \cos \frac{2\pi j}{n} \quad \text{and} \quad (\bar{\mathbf{v}}_2)_j := \sin \frac{2\pi j}{n}.$$

The coefficients  $\mathbf{v}_k$  of the basis functions  $f_{\mathbf{v}_k}$  (3) are then computed from  $\bar{\mathbf{v}}_1$  and  $\bar{\mathbf{v}}_2$  as

$$\begin{aligned} \mathbf{v}_0 &:= \mathbf{1} \diamond \mathbf{1} \in \mathcal{P}_6, & \mathbf{v}_3 &:= \bar{\mathbf{v}}_1 \diamond \bar{\mathbf{v}}_1 + \bar{\mathbf{v}}_2 \diamond \bar{\mathbf{v}}_2, \\ \mathbf{v}_1 &:= \bar{\mathbf{v}}_1 \diamond \mathbf{1}, & \mathbf{v}_4 &:= \bar{\mathbf{v}}_1 \diamond \bar{\mathbf{v}}_1 - \bar{\mathbf{v}}_2 \diamond \bar{\mathbf{v}}_2, \\ \mathbf{v}_2 &:= \bar{\mathbf{v}}_2 \diamond \mathbf{1}, & \mathbf{v}_5 &:= 2\bar{\mathbf{v}}_1 \diamond \bar{\mathbf{v}}_2. \end{aligned} \quad (4)$$

## 6. $C^2$ Polar Spline Construction

This section defines the polar spline  $h_{\mathbf{b}}(r, \gamma)$  algorithmically. We determine the control points  $\mathbf{b}_{ij} \in \mathbb{R}^3$ , separately for each  $x, y$  or  $z$ -coordinate  $\mathbf{b}_{ij} \in \mathbb{R}$  as linear expressions in  $\mathbf{p}_k \mathbf{v}_k, k = 0, \dots, 5$ . Here  $\mathbf{v}_k$  defines the periodic behavior of the spline, while  $\mathbf{p}_k \in \mathbb{R}$  represents the quadratic radial expansion derived from the polar configuration.

*Input: A 2-layer polar configuration*

Fig. 6a shows a 2-layer polar configuration defining the polar cap.

*Output: One bivariate periodic spline  $h_{\mathbf{b}} \in \mathcal{S}$*

Fig. 6c labels the coefficients

$$\mathbf{b}_{ij} \in \mathbb{R} \quad \text{for } i \in \{0, 1, \dots, 6\} \text{ and } j \in \mathbb{Z}_{4n}$$

of one coordinate of the  $C^2$  polar spline. The polar spline is a single tensor-product spline patch  $h_{\mathbf{b}}(r, \gamma)$  of degree  $(3, 6)$ . Its knots are  $[0, 0, 0, 0, 1, 2, 3, 4, 5, 6, 7]$  in the radial parameter  $r$  and are uniformly-spaced 4-fold knots in the periodic parameter  $\gamma$ .

*Algorithm*

**Step 0.** We apply the masks of Appendix B to refine the input 2-layers to a 4-layer polar configuration with  $6n$  vertices

$$(\mathbf{q}_{ij})_{i \in \{0, 1, \dots, 5\}, j \in \mathbb{Z}_n} \quad (\text{per coordinate: } \mathbf{q}_{ij})$$

that are indexed by  $i$  in the radial direction and by  $j$  in the periodic direction as shown in Fig. 6b. The polar vertex  $\mathbf{q}_{0j} := \mathbf{q}_{00}$  is replicated  $n$  times.

**Step 1.** Compute  $\mathbf{v}_k \in \mathcal{P}_6$  by (4).

**Step 2.** Let  $c_\gamma := \cos(2\pi\gamma)$  and  $s_\gamma := \sin(2\pi\gamma)$  and  $\mathbf{q}_{ij}$  one coordinate of the output from Step 0. Then compute

$$\begin{aligned} \mathbf{p}_0 &:= \frac{2}{3} \mathbf{q}_{00} + \frac{1}{3n} \sum_{j=0}^{n-1} \mathbf{q}_{1j}, & \mathbf{p}_3 &:= -\mathbf{q}_{00} + \frac{1}{n} \sum_{j=0}^{n-1} \mathbf{q}_{1j}, \\ \mathbf{p}_1 &:= \frac{2}{n} \sum_{j=0}^{n-1} c_{j/n} \mathbf{q}_{1j}, & \mathbf{p}_4 &:= \frac{2}{n} \sum_{j=0}^{n-1} c_{2j/n} \mathbf{q}_{1j} \in \mathbb{R} \\ \mathbf{p}_2 &:= \frac{2}{n} \sum_{j=0}^{n-1} s_{j/n} \mathbf{q}_{1j}, & \mathbf{p}_5 &:= \frac{2}{n} \sum_{j=0}^{n-1} s_{2j/n} \mathbf{q}_{1j}. \end{aligned} \quad (5)$$

**Step 3.** For each coordinate, form the spline's coefficients

$$\begin{aligned} \mathbf{b}_{0\circ} &:= \mathbf{p}_0 \mathbf{v}_0 & \in \mathcal{P}_6 \\ \mathbf{b}_{1\circ} &:= \mathbf{p}_0 \mathbf{v}_0 + \frac{1}{3} (\mathbf{p}_1 \mathbf{v}_1 + \mathbf{p}_2 \mathbf{v}_2) \\ \mathbf{b}_{2\circ} &:= \mathbf{p}_0 \mathbf{v}_0 + (\mathbf{p}_1 \mathbf{v}_1 + \mathbf{p}_2 \mathbf{v}_2) + \frac{2}{3} (\mathbf{p}_3 \mathbf{v}_3 + \mathbf{p}_4 \mathbf{v}_4 + \mathbf{p}_5 \mathbf{v}_5) \\ \mathbf{b}_{i\circ} &:= \mathbf{q}_{i-1, \circ} \diamond \mathbf{1} \quad \text{for } i \in \{3, 4, 5, 6\}. \end{aligned} \quad (6)$$

Since  $\mathbf{v}_0$  is a vector of all 1s,  $\mathbf{b}_{0\circ}$  is collapsed to the single point  $\mathbf{p}_0$  so that the pole is well-defined.

*Comments* Step 0 can be omitted if there is no other extraordinary or polar vertex in the 4-link. Then the 4-link can be used directly. The values computed in Step 1 can be pre-computed for a range of  $n$  so that the step can be omitted. The choice of  $\mathbf{p}_k$  in Step 2 is explained in Section 8:  $\mathbf{p}_1, \mathbf{p}_2, \mathbf{p}_4$ , and  $\mathbf{p}_5$  are computed using the discrete Fourier transform in the periodic direction, while the formulas for  $\mathbf{p}_0$  and  $\mathbf{p}_3$  emulate cubic B-spline knot-insertion in the radial direction. Step 3 defines the innermost  $i$ -links  $\mathbf{b}_{0\circ}, \mathbf{b}_{1\circ}$ , and  $\mathbf{b}_{2\circ}$  of the quadratic expansion (2) at the pole. The outer  $i$ -links  $\mathbf{b}_{3\circ}, \mathbf{b}_{4\circ}, \mathbf{b}_{5\circ}, \mathbf{b}_{6\circ}$ , are degree-raised  $i$ -links of the polar configuration.

## 7. Proof of curvature continuity

$C^2$  continuity between the output spline  $h_{\mathbf{b}}$  and surrounding bi-3 splines is straightforward since, by (6), the control points  $\mathbf{b}_{3\circ}, \dots, \mathbf{b}_{6\circ}$  define the same surface (in degree-raised form) as  $\mathbf{q}_{2\circ}, \dots, \mathbf{q}_{5\circ}$ . Therefore  $h_{\mathbf{b}}$  is bi-3  $C^2$  compatible as claimed.

To prove curvature continuity at the pole  $h_{\mathbf{b}}(0,0)$ , we derive an explicit expansion at the pole.

**Theorem 1.** *The polar spline  $h_{\mathbf{b}}$  is  $C^2$  at the pole.*

*Proof.* We show that, at  $(0,0)$ , the spline  $h_{\mathbf{b}}(r, \gamma)$  differs from a quadratic map  $\tilde{h}(r, \gamma)$  by  $o(r^2)$  in the radial parameter  $r$ .

We define  $\tilde{h}(r, \gamma)$  as a spline of degree (3, 6):

$$\tilde{h}(r, \gamma) := \sum_{k=0}^5 \mathbf{p}_k f_{\mathbf{v}_k}(\gamma) g_{\mathbf{u}_k}(r), \quad (7)$$

where  $\mathbf{p}_k$  is defined by (5),  $\mathbf{v}_k \in \mathcal{P}_6$  by (4),  $f_{\mathbf{v}_k}$  by (3),

$$\begin{aligned} \mathbf{u}_0 &:= [1, 1, 1, 1, 1, 1], \\ \mathbf{u}_1 &:= \mathbf{u}_2 := [0, \frac{1}{3}, 1, 2, 3, 4, 5], \\ \mathbf{u}_3 &:= \mathbf{u}_4 := \mathbf{u}_5 := \frac{1}{3}[0, 0, 2, 11, 26, 47, 74], \end{aligned} \quad (8)$$

and  $g_{\mathbf{u}_k}(r)$  is the univariate  $C^2$  degree-3 spline with coefficient vector  $\mathbf{u}_k$  and knots  $[0, 0, 0, 0, 1, 2, 3, 4, 5, 6, 7]$ . By this choice of  $\mathbf{u}_k$ ,

$$\begin{aligned} g_{\mathbf{u}_0}(r) &= 1, \\ g_{\mathbf{u}_1}(r) &= g_{\mathbf{u}_2}(r) = r, \\ g_{\mathbf{u}_3}(r) &= g_{\mathbf{u}_4}(r) = g_{\mathbf{u}_5}(r) = r^2, \end{aligned} \quad (9)$$

so that  $\tilde{h}(r, \gamma)$  represents the quadratic expansion (2) as is evident after the change of variables  $(x, y) := (r f_{\mathbf{v}_1}(\gamma), r f_{\mathbf{v}_2}(\gamma))$  suggested in Table 1(b,c):

$$\begin{aligned} \tilde{h}(r, \gamma) &\stackrel{(9)}{=} \mathbf{p}_0 + r(\mathbf{p}_1 f_{\mathbf{v}_1}(\gamma) + \mathbf{p}_2 f_{\mathbf{v}_2}(\gamma)) \\ &\quad + r^2(\mathbf{p}_3 f_{\mathbf{v}_3}(\gamma) + \mathbf{p}_4 f_{\mathbf{v}_4}(\gamma) + \mathbf{p}_5 f_{\mathbf{v}_5}(\gamma)) \\ &\stackrel{(4)}{=} \mathbf{p}_0 + r(\mathbf{p}_1 f_{\mathbf{v}_1}(\gamma) + \mathbf{p}_2 f_{\mathbf{v}_2}(\gamma)) + r^2(\mathbf{p}_3 (f_{\mathbf{v}_1}(\gamma)^2 + f_{\mathbf{v}_2}(\gamma)^2) \\ &\quad + \mathbf{p}_4 (f_{\mathbf{v}_1}(\gamma)^2 - f_{\mathbf{v}_2}(\gamma)^2) + \mathbf{p}_5 (2f_{\mathbf{v}_1}(\gamma)f_{\mathbf{v}_2}(\gamma))) \\ &= \mathbf{p}_0 + \mathbf{p}_1 x + \mathbf{p}_2 y + \mathbf{p}_3 (x^2 + y^2) + \mathbf{p}_4 (x^2 - y^2) + \mathbf{p}_5 (2xy). \end{aligned}$$

The first three formulas in (6) may be rewritten as follows.

$$\begin{bmatrix} \mathbf{b}_{0\circ} \\ \mathbf{b}_{1\circ} \\ \mathbf{b}_{2\circ} \end{bmatrix} = \begin{bmatrix} 1 & 0 & 0 \\ 1 & \frac{1}{3} & 0 \\ 1 & 1 & \frac{2}{3} \end{bmatrix} \begin{bmatrix} \mathbf{p}_0 \mathbf{v}_0 \\ \mathbf{p}_1 \mathbf{v}_1 + \mathbf{p}_2 \mathbf{v}_2 \\ \mathbf{p}_3 \mathbf{v}_3 + \mathbf{p}_4 \mathbf{v}_4 + \mathbf{p}_5 \mathbf{v}_5 \end{bmatrix}.$$

Since the columns of the matrix agree with  $\mathbf{u}_k$ , it is clear that the pole-most three  $i$ -links of  $h_{\mathbf{b}}$  agree with those of  $\tilde{h}$ . Consequently,  $h_{\mathbf{b}}(r, \gamma) = \tilde{h}(r, \gamma) + o(r^2)$  and the quadratic expansion of  $h_{\mathbf{b}}(r, \gamma)$  matches that of  $\tilde{h}(r, \gamma)$  at  $(0,0)$ .  $\square$  For generic input data, the polar spline cap with coordinates  $h_{\mathbf{b}}$  therefore has a  $C^2$  embedding at the pole.

## 8. Mapping a polar configuration $\mathbf{q}$ to the quadratic expansion coefficients $\mathbf{p}_k$

Theorem 1 does not depend on the choice of the six coefficients  $\mathbf{p}_k$  that define the geometry of the quadratic expansion at pole. Our choice (5) of the  $\mathbf{p}_k$  represents a natural projection from the polar configuration.

Since each function in  $\mathbf{s}$  corresponds to precisely one Fourier frequency in the periodic direction (cf. Table 1d), it is natural to match these frequencies, by having the formulas for  $\mathbf{p}_k$ ,  $k \in \{1, 2, 4, 5\}$  match the discrete Fourier transforms of the 1-link  $\mathbf{q}_{1\circ}$ .

Since the Fourier transform of the 1-link only prescribes an average and does not include a contribution from the polar vertex  $\mathbf{q}_{00}$ , the formulas for  $\mathbf{p}_0$  and  $\mathbf{p}_3$  are derived to mimic knot-insertion into a uniform cubic B-spline in the radial direction. To see this, we consider the limit as  $n \rightarrow \infty$  and interpret the dense set of control points as a function of  $\gamma$  (see Fig. 7). For simplicity, we consider an initial control mesh  $\mathbf{q}_{1\circ}$  that is symmetric under rotation about the axis through  $\mathbf{q}_{00}$  and  $\text{avg}_{\gamma}(\mathbf{q}_{1\gamma})$ , the average (centroid) of the dense set of 1-link control points. Then  $\mathbf{p}_4 = \mathbf{p}_5 = 0$  and

$$f_{\mathbf{b}_{1\circ}}(\gamma) \stackrel{(6)}{=} \mathbf{p}_0 + \frac{1}{3}(\mathbf{p}_1 c_{\gamma} + \mathbf{p}_2 s_{\gamma}), \quad (10)$$

$$\begin{aligned} f_{\mathbf{b}_{2\circ}}(\gamma) &\stackrel{(6)}{=} \mathbf{p}_0 + \mathbf{p}_1 c_{\gamma} + \mathbf{p}_2 s_{\gamma} + \frac{2}{3} \left( \mathbf{p}_3 + \cancel{\mathbf{p}_4 c_{2\gamma}} + \cancel{\mathbf{p}_5 s_{2\gamma}} \right) \\ &= \mathbf{p}_0 + \mathbf{p}_1 c_{\gamma} + \mathbf{p}_2 s_{\gamma} + \frac{2}{3} \mathbf{p}_3. \end{aligned} \quad (11)$$

We now focus on one radial slice with fixed angle  $\gamma$ . Due to density,  $f_{\mathbf{q}_{1\circ}}(\gamma - \frac{1}{2})$  is well-defined, we can consider control points  $[f_{\mathbf{q}_{1\circ}}(\gamma - \frac{1}{2}), f_{\mathbf{q}_{0\circ}}(\gamma), f_{\mathbf{q}_{1\circ}}(\gamma), f_{\mathbf{q}_{2\circ}}(\gamma), f_{\mathbf{q}_{3\circ}}(\gamma)]$  of a radial cubic spline with knots  $[-3, -2, -1, 0, 1, 2, 3, 4, 5]$  (Fig. 7a). We define  $\mathbf{p}$  and hence  $\mathbf{b}$  by 3-fold knot insertion at 0:

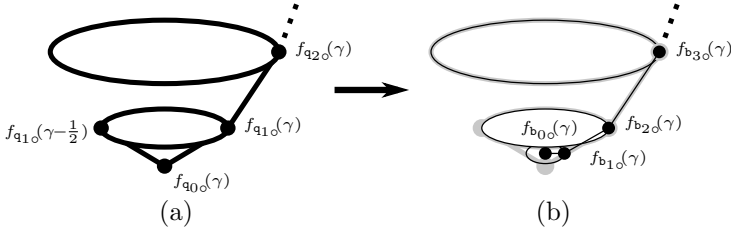


Fig. 7. **Knot insertion analogy.** The conversion of a symmetric (infinite-valent) polar configuration  $\mathbf{q}$  to spline control points  $\mathbf{b}$  corresponds to knot insertion in the radial direction.

$$\begin{aligned} f_{b_{0o}}(\gamma) &= \frac{1}{6} \left( f_{q_{1o}}(\gamma - \frac{1}{2}) + 4f_{q_{0o}}(\gamma) + f_{q_{1o}}(\gamma) \right), \\ f_{b_{1o}}(\gamma) &= \frac{2}{3}f_{q_{0o}}(\gamma) + \frac{1}{3}f_{q_{1o}}(\gamma), \\ f_{b_{2o}}(\gamma) &= f_{q_{1o}}(\gamma), \quad f_{b_{3o}}(\gamma) = f_{q_{2o}}(\gamma), \quad f_{b_{4o}}(\gamma) = f_{q_{3o}}(\gamma). \end{aligned} \quad (12)$$

$$(13)$$

Then

$$\begin{aligned} \mathbf{p}_0 &\stackrel{(10)}{=} \text{avg}_\gamma(f_{b_{1o}}(\gamma)) \\ &\stackrel{(12)}{=} \frac{2}{3}f_{q_{0o}}(\gamma) + \frac{1}{3}\text{avg}_\gamma(f_{q_{1o}}(\gamma)) \end{aligned} \quad (14)$$

and

$$\begin{aligned} f_{b_{1o}}(\gamma) &\stackrel{(12)}{\stackrel{(13)}{=}} \frac{2}{3}f_{q_{0o}}(\gamma) + \frac{1}{3}f_{b_{2o}}(\gamma) \\ &\stackrel{(10)}{\stackrel{(11)}{\Rightarrow}} \mathbf{p}_0 + \frac{1}{3}(\mathbf{p}_1 c_\gamma + \mathbf{p}_2 s_\gamma) = \frac{2}{3}f_{q_{0o}}(\gamma) \\ &\quad + \frac{1}{3} \left( \mathbf{p}_0 + \mathbf{p}_1 c_\gamma + \mathbf{p}_2 s_\gamma + \frac{2}{3}\mathbf{p}_3 \right) \\ \Rightarrow \mathbf{p}_3 &= 3(\mathbf{p}_0 - f_{q_{0o}}(\gamma)) \stackrel{(14)}{=} -f_{q_{0o}}(\gamma) + \text{avg}_\gamma(f_{q_{1o}}(\gamma)). \end{aligned}$$

This yields the choice of  $\mathbf{p}_0$  and  $\mathbf{p}_3$  in (5).

## 9. The relation of Polar Splines to Subdivision

A 2-layer polar configuration can be directly converted into a  $C^1$  bi-3 spline cap such that  $\mathbf{p}_1$  and  $\mathbf{p}_2$  span the tangent plane at the pole  $\mathbf{p}_0$ . We use this fact to illustrate the relation of polar splines to subdivision. Improving on [MKP08], this  $C^1$  construction does not require an initial subdivision of the polar configuration: it yields equally good shape with fewer control points since  $\mathbf{p}_k$  are derived using the knot-insertion analogy in Section 8.

**Lemma 1.** *The bi-3 spline with knots  $[0, 0, 0, 0, 1, 2, 3, 4, 5]$  in the radial and  $\frac{1}{n}\mathbb{Z}_n$  in the periodic direction and control points  $(\bar{\mathbf{b}}_{ij})_{i \in \{0,1,\dots,4\}, j \in \mathbb{Z}_n}$  (cf. Fig. 8),*

$$\begin{aligned} \bar{\mathbf{b}}_{0o} &:= \mathbf{p}_0 \mathbf{1} \\ \bar{\mathbf{b}}_{1o} &:= \mathbf{p}_0 \mathbf{1} + \frac{1}{3}(\mathbf{p}_1 \bar{\mathbf{v}}_1 + \mathbf{p}_2 \bar{\mathbf{v}}_2) \\ \bar{\mathbf{b}}_{io} &:= \mathbf{q}_{i-1,o} \quad \text{for } i \in \{2, 3, 4\}, \end{aligned} \quad (15)$$

*forms a  $C^1$  surface with bounded curvature, unless the  $\bar{\mathbf{b}}_{ij}$  are in special position.*

Excluding control nets in ‘special position’ avoids discussing degenerate embeddings. The proof of tangent continuity and bounded curvature at the pole is identical to

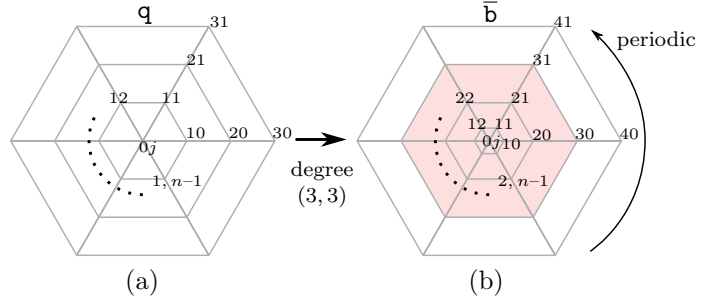


Fig. 8. A  $C^1$  **polar spline.** (a) A 2-layer polar configuration  $\mathbf{q}$  can be converted without an intermediate subdivision step to (b) a bi-3 spline  $h_{\bar{\mathbf{b}}}$  defined by control points  $\bar{\mathbf{b}}$  (in the central pink region).

that in [MKP08] since the 1-link  $\bar{\mathbf{b}}_{1o}$  lies in *oval position*, i.e. satisfies for some point  $\mathbf{o}$  and vectors  $\mathbf{e}_1, \mathbf{e}_2$ ,

$$\bar{\mathbf{b}}_{1j} = \mathbf{o} + \mathbf{e}_1 c_{j/n} + \mathbf{e}_2 s_{j/n}, \quad c_{j/n} := \cos \frac{2\pi j}{n}.$$

*Proof.* We interpret  $\bar{\mathbf{b}}$  as a polar subdivision control mesh, enumerated as a column vector, and devise a subdivision matrix  $\bar{A}$  which composes the effect of

- (i) inserting knots along the radial direction at the half integers, so that the radial knot sequence  $[0, 0, 0, 0, 1, 2, 3, 4, 5]$  is transformed to  $\frac{1}{2}[0, 0, 0, 0, 1, 2, 3, 4, 5]$ ; and
- (ii) projecting the 1-link into oval position.

Once the 1-link is in oval position, step 2 above has no impact since radial knot insertion preserves the oval position. Essentially,  $\bar{A}\bar{\mathbf{b}} \in \mathcal{S}_3$  reparameterizes  $h_{\bar{\mathbf{b}}}$  so that  $h_{\bar{\mathbf{b}}}(\frac{1}{2}r, \gamma) = h_{\bar{A}\bar{\mathbf{b}}}(r, \gamma)$ . Spectral analysis of this subdivision algorithm then establishes bounded curvature at the pole  $h_{\bar{\mathbf{b}}}(0, \gamma)$ .  $\square$

A similar auxiliary  $C^2$  subdivision algorithm can be defined to yield the  $C^2$  polar spline  $h_{\bar{\mathbf{b}}}$ . Its matrix  $A$  inserts knots in the radial direction and projects the resulting 1- and 2-links to satisfy the relationships (6). Spectral analysis of  $A$  yields the dominant six eigenvalues  $(\lambda_0, \lambda_1, \lambda_2, \lambda_3, \lambda_4, \lambda_5) := (1, \lambda, \lambda, \lambda^2, \lambda^2, \lambda^2)$  where  $\lambda := \frac{1}{2}$ . The corresponding eigenvectors  $\mathbf{w}_k, k \in \{0, \dots, 5\}$ , are

$$(\mathbf{w}_k)_{ij} := (\mathbf{u}_k)_i (\mathbf{v}_k)_j, \quad i \in \{0, \dots, 6\}, j \in \{0, \dots, 4n\} \quad (16)$$

( $\mathbf{u}_k$  from (8) and  $\mathbf{v}_k$  from (4)). As shown in Table 1, the corresponding splines satisfy the  $C^2$  conditions in Theorem 7.16 of [PR08]

$$\{h_{\mathbf{w}_3}, h_{\mathbf{w}_4}, h_{\mathbf{w}_5}\} \in \text{span}\{h_{\mathbf{w}_1}^2, h_{\mathbf{w}_2}^2, h_{\mathbf{w}_1} h_{\mathbf{w}_2}\}. \quad (17)$$

An alternative interpretation of our choice of  $\mathbf{w}_k$  is therefore that we construct the spline so that its associated subdivision algorithm matches the  $C^2$  conditions.

Conversely, subdivision theory prescribes a minimal generic degree of the  $C^2$  polar spline (see Section 3 and Figure 4): since  $C^2$  continuity in the periodic direction requires periodic degree at least 3,  $h_{\mathbf{w}_1}$  and  $h_{\mathbf{w}_2}$  must have degree at least (1, 3) and, by (17), the degree is at least (2, 6) for  $h_{\mathbf{w}_3}, h_{\mathbf{w}_4}$ , and  $h_{\mathbf{w}_5}$ . To model higher-order (mon-key) saddles, radial degree 3 is needed. In that sense, our degree (3, 6) is optimal.

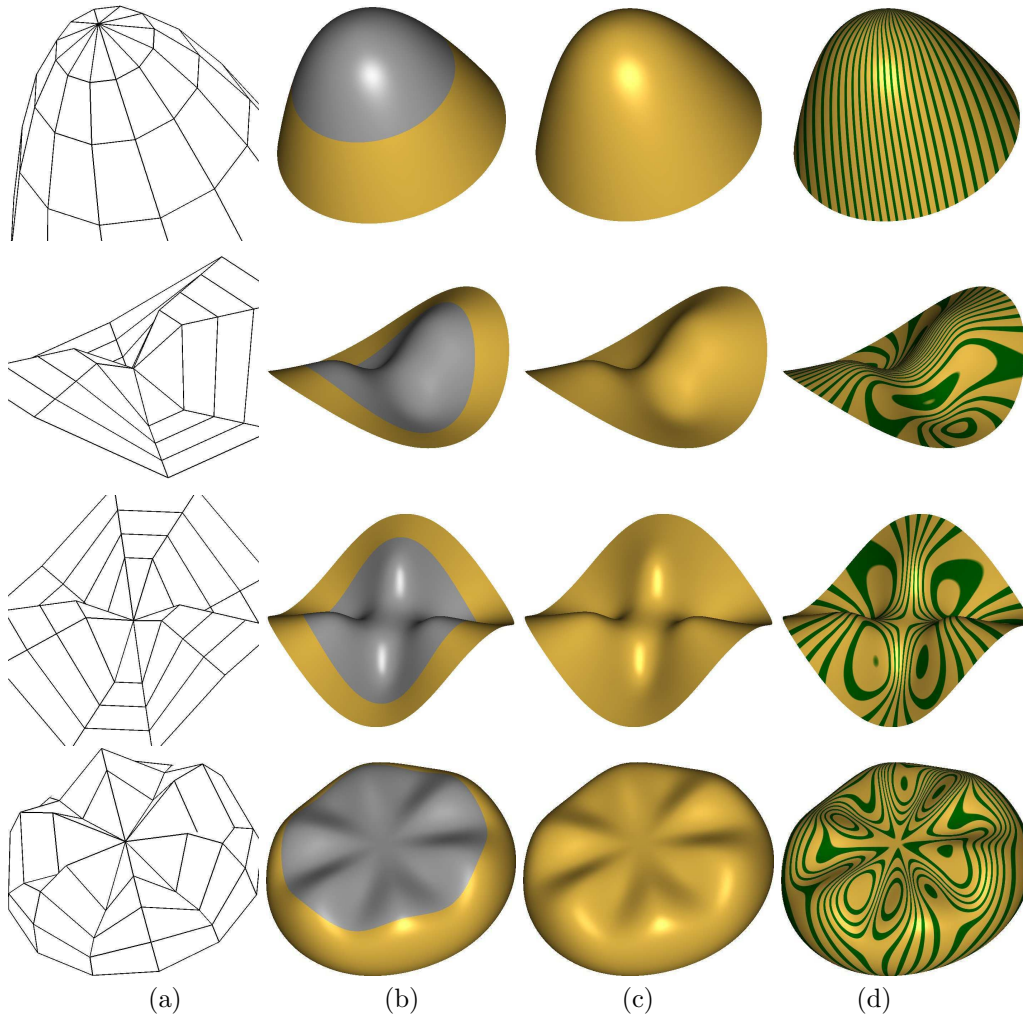


Fig. 9. **Shape Trials.** (a) Each embedded polar configuration defines (b) a  $C^2$  polar spline of degree (3, 6) (gray) surrounded by a bicubic spline ring (gold); (c) shows the ensemble. (d) Highlight lines show smoothness of the transition from the bicubic neighborhood to the pole.

## 10. Results and Discussion

The test cases Fig. 9 and 10 illustrate the shape properties of  $C^2$  polar splines over the first few modes of oscillation. We would like the surface to have low fluctuations in the distribution of Gaussian curvature and of the highlight lines; and it should continue shape from the boundary data without abrupt changes. The comparison in Fig. 10 shows that a  $C^2$  polar spline cap behaves qualitatively no different from its subdivision counterparts [KMP06,MKP08] even though it consists of just one spline patch.

To illustrate that  $C^2$  polar splines are *bi-3*  $C^2$  compatible, Fig. 11 shows the interplay between regions defined by standard  $C^2$  bi-3 tensor-product splines (gold in (c)), polar splines (grey in (c)), and regions covered with a hole filling algorithm for extraordinary vertices (green in (c)). The Tee in Fig. 11 and the Chair in Fig. 2 have Catmull-Clark extraordinary vertices in the 3-link of a polar vertex so that the output of a bi-3 compatible algorithm joins directly with the polar spline. While it is possible to adapt  $C^2$  polar splines to allow for extraordinary vertices in the

2-link, it is preferable to have the designer introduce a separating edge-loop to unambiguously define the  $C^2$  bi-3 transition between polar splines and bi-3  $C^2$  compatible splines. This also avoids having to modify existing algorithms [Pra97,KP09b,LS08] that expect a full quad neighborhood around extraordinary vertices.

The coefficients  $\mathbf{p}_k$  correspond to intuitive geometric properties of the surface illustrated in Fig. 3. They can be adjusted by the user via the polar configuration control points or even directly to meet design constraints – without affecting the smoothness of the resulting spline surface.

To generalize the approach of this paper to  $C^K$  surfaces of degree  $(K+1, K(K+1))$  at the pole, we need only choose functions  $h_{\mathbf{w}_k}$  that span the  $K^{\text{th}}$  order Taylor expansion. The quality of the construction will then depend on the choice of coefficients  $\mathbf{p}_k$ .

## Acknowledgements

This work was supported by the National Science Foundation Grant 0728797.

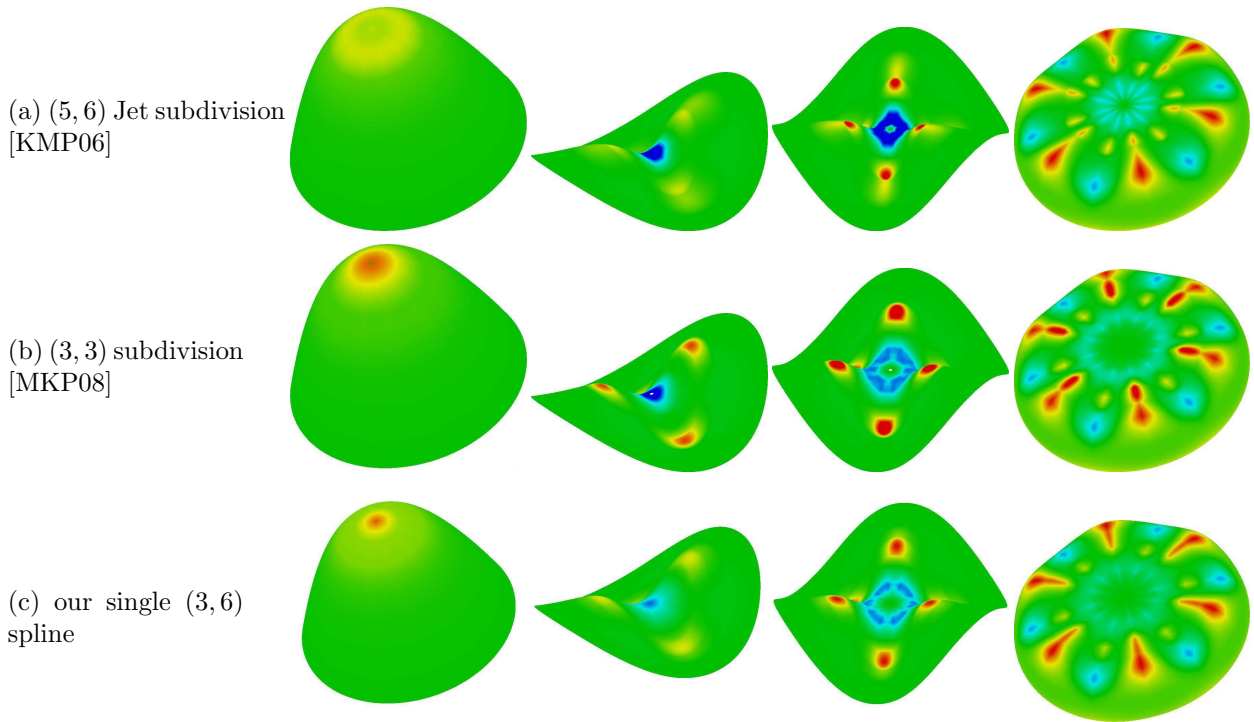


Fig. 10. **Curvature comparison** of  $C^2$  Polar Jet Subdivision [KMP06], Bi-3  $C^2$  Polar Subdivision [MKP08], and our method. The Gauss curvature ranges from *blue* (negative) to *green* (near 0) to *red* (positive).

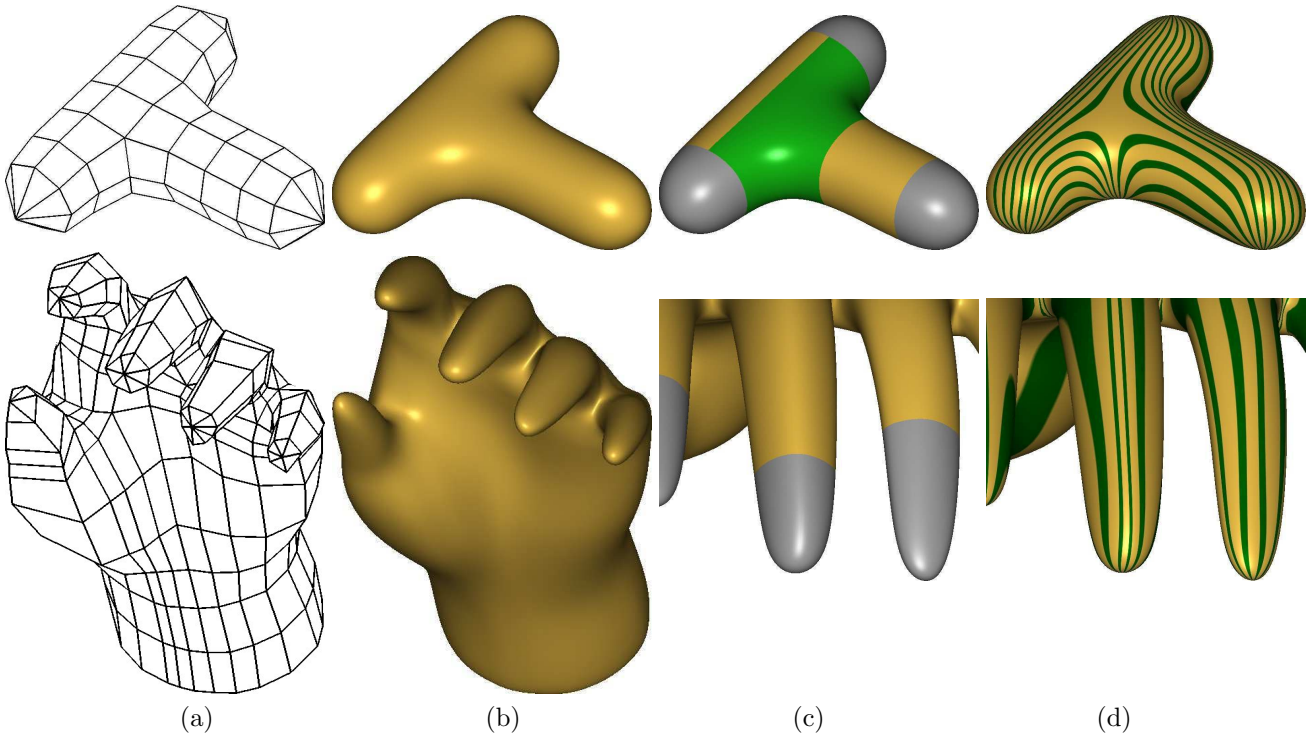


Fig. 11. **The “Tee” and finger tips.** (a) A quad mesh with polar configurations defines (b) the spline surface consisting of (c) uniform bicubics (*gold*),  $C^2$  polar splines (*gray*), and bi-3 compatible schemes like [Pra97,Pet02,LS08] (*green*) that fill holes caused by extraordinary vertices. (d) The highlight lines flow smoothly across poles and the boundary of the polar spline.

### Appendix A. Multiplying uniform cubic splines

The product of two uniform cubics is a sextic spline with 4-fold knots. To form the product, we convert the cubics

to Bézier form, multiply, and remove two knots at every breakpoint of the resulting spline of degree 6.

- (i) A uniform spline with control points  $[a_0, a_1, a_2, a_3]$  has Bézier control points

- $\frac{1}{6}[a_0+4a_1+a_2, 4a_1+2a_2, 2a_1+4a_2, a_1+4a_2+a_3]$ .
- (ii) Multiplying a pair of cubic polynomials with Bézier control points  $[b_0, b_1, b_2, b_3]$  and  $[\hat{b}_0, \hat{b}_1, \hat{b}_2, \hat{b}_3]$  yields degree 6 control points  $c := [b_0\hat{b}_0, \frac{1}{2}b_0\hat{b}_1 + \frac{1}{2}b_1\hat{b}_0, \frac{1}{5}b_0\hat{b}_2 + \frac{3}{5}b_1\hat{b}_1 + \frac{1}{5}b_2\hat{b}_0, \frac{1}{20}b_0\hat{b}_3 + \frac{9}{20}b_1\hat{b}_2 + \frac{9}{20}b_2\hat{b}_1 + \frac{1}{20}b_3\hat{b}_0, \frac{1}{5}b_1\hat{b}_3 + \frac{3}{5}b_2\hat{b}_2 + \frac{1}{5}b_3\hat{b}_1, \frac{1}{2}b_2\hat{b}_3 + \frac{1}{2}b_3\hat{b}_2, b_3\hat{b}_3]$
- (iii) Two knots are removed from both ends of the degree-6 Bézier form to obtain the  $C^2$  spline of degree 6 by the following sequence of operations ( $\leftarrow$  indicates assignment).

remove knots once

$$c_0 \leftarrow 2c_0 - c_1, \quad c_6 \leftarrow 2c_6 - c_5$$

remove knots again

$$c_1 \leftarrow 2c_1 - c_2, \quad c_5 \leftarrow 2c_5 - c_4$$

$$c_0 \leftarrow 2c_0 - c_1, \quad c_6 \leftarrow 2c_6 - c_5$$

Combining these three steps, an explicit formula was derived and is implemented by the following C++ procedure.

```
// Multiply two uniform periodic degree 3 splines with
// n control points each to yield a single degree 6 spline
// with 4n control points and 4-fold knot multiplicity.
template <typename T1, typename T2>
void bsp_mul33(int n, const T1 a[], const T2 b[], T1 c[])
{
  for (int i = 0; i < n; ++i) {
    int im1 = (i-1+n)%n;
    int ip1 = (i+1)%n;
    int ip2 = (i+2)%n;
    const T1 &a0 = a[im1]; const T1 &a1 = a[i];
    const T1 &a2 = a[ip1]; const T1 &a3 = a[ip2];
    const T2 &b0 = b[im1]; const T2 &b1 = b[i];
    const T2 &b2 = b[ip1]; const T2 &b3 = b[ip2];
    c[4*i+0] = a0*b1/10.0 + a0*b2/30.0 + a1*b0/10.0
              + 8.0/15.0*a1*b1 + a1*b2/10.0
              + a2*b0/30.0 + a2*b1/10.0;
    c[4*i+1] = a0*b1/90.0 + a0*b2/45.0 + 16.0/45.0*a1*b1
              + 7.0/30.0*a1*b2 + 7.0/30.0*a2*b1
              + a2*b2/9.0 + a1*b0/90.0 + a2*b0/45.0;
    c[4*i+2] = a0*b3/720.0 + a1*b3/180.0 + a2*b3/720.0
              + a0*b1/720.0 + a0*b2/180.0 + a1*b0/720.0
              + 19.0/90.0*a1*b1 + 197.0/720.0*a1*b2
              + a2*b0/180.0 + 197.0/720.0*a2*b1
              + 19.0/90.0*a2*b2 + a3*b0/720.0
              + a3*b1/180.0 + a3*b2/720.0;
    c[4*i+3] = a1*b1/9.0 + 7.0/30.0*a1*b2 + a1*b3/45.0
              + 7.0/30.0*a2*b1 + 16.0/45.0*a2*b2
              + a2*b3/90.0 + a3*b1/45.0 + a3*b2/90.0;
  }
}
```

## Appendix B. Masks for Step 0

Step 0 of the a  $C^2$  polar spline construction (Figure 6) refines the polar configuration according to [MKP08], i.e. with the masks of Fig. B.1 and

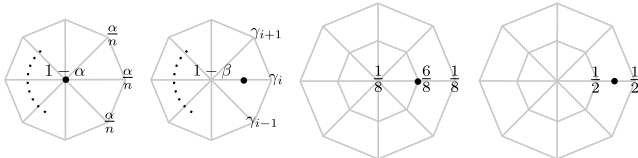


Fig. B.1. Refinement rules for Step 0 (from [MKP08]).

$$\alpha := \beta - \frac{1}{4}, \quad \beta := \frac{5}{8}, \quad c_\gamma := \cos(2\pi\gamma),$$

$$\gamma_k := \frac{1}{n} \left( \beta - \frac{1}{2} + \frac{5}{8}c_{k/n} + (c_{k/n})^2 + \frac{1}{2}(c_{k/n})^3 \right).$$

## References

- [BR97] BOHL H., REIF U.: Degenerate Bézier patches with continuous curvature. *Comput. Aided Geom. Des.* 14, 8 (1997), 749–761.
- [KMP06] KARČIAUSKAS K., MYLES A., PETERS J.: A  $C^2$  polar jet subdivision. In *Symposium on Geometry Processing* (2006), Eurographics Association, pp. 173–180.
- [KP07a] KARČIAUSKAS K., PETERS J.: Surfaces with polar structure. *Computing* 79 (March 2007), 309–315.
- [KP07b] KARČIAUSKAS K., PETERS J.: Concentric tessellation maps and curvature continuous guided surfaces. *Comput. Aided Geom. Des.* 24, 2 (2007), 99–111.
- [KP09a] KARČIAUSKAS K., PETERS J.: Finite curvature continuous polar patchworks. In *IMA Mathematics of Surfaces XIII Conference* (2009), Hancock E., Martin R., Sabin M., (Eds.), pp. 222–234.
- [KP09b] KARČIAUSKAS K., PETERS J.: Guided spline surfaces. *Computer Aided Geometric Design* 26, 1 (2009), 105–116.
- [Lev06] LEVIN A.: Modified subdivision surfaces with continuous curvature. In *SIGGRAPH '06: ACM SIGGRAPH 2006 Papers* (New York, NY, USA, 2006), ACM Press, pp. 1035–1040.
- [Loo04] LOOP C. T.: Second order smoothness over extraordinary vertices. In *Symposium on Geometry Processing* (New York, NY, USA, 2004), ACM, pp. 165–174.
- [LS08] LOOP C. T., SCHAEFER S.:  $G^2$  tensor product splines over extraordinary vertices. *Computer Graphics Forum (Proceedings of 2008 Symposium on Geometry Processing)* 27, 5 (2008), 1373–1382.
- [MKP08] MYLES A., KARČIAUSKAS K., PETERS J.: Pairs of bi-cubic surface constructions supporting polar connectivity. *Comput. Aided Geom. Des.* 25, 8 (2008), 621–630.
- [MP09] MYLES A., PETERS J.: Bi-3  $C^2$  polar subdivision. *ACM Trans. Graph.* 28, 3 (Aug 2009), 1–12.
- [Pet02] PETERS J.:  $C^2$  free-form surfaces of degree (3,5). *Comput. Aided Geom. Des.* 19, 2 (2002), 113–126.
- [PR08] PETERS J., REIF U.: *Subdivision Surfaces*. Geometry and Computing, Vol. 3. Springer-Verlag New York, Inc., New York, NY, USA, Apr 2008.
- [Pra97] PRAUTZSCH H.: Freeform splines. *Comput. Aided Geom. Des.* 14, 3 (1997), 201–206.
- [Rei98] REIF U.: TURBS—topologically unrestricted rational B-splines. *Constructive Approximation. An International Journal for Approximations and Expansions* 14, 1 (1998), 57–77.
- [YZ04] YING L., ZORIN D.: A simple manifold-based construction of surfaces of arbitrary smoothness. *ACM Trans. Graph.* 23, 3 (Aug. 2004), 271–275.
- [Zor06] ZORIN D.: Constructing curvature-continuous surfaces by blending. In *Symposium on Geometry Processing* (2006), Eurographics Association, pp. 31–40.